

# A Free Wake Linear Inflow Model Extraction Procedure for Rotorcraft Analysis

**Jeffrey D. Keller**  
Senior Associate

**Robert M. McKillip, Jr.**  
Senior Associate  
Continuum Dynamics, Inc.  
Ewing, NJ, USA

**Daniel A. Wachspress**  
Senior Associate

**Mark B. Tischler**  
Senior Technologist  
Group Leader, Flight Control Technology  
US Army Aviation Development Directorate (AMRDEC)  
Moffett Field, CA, USA

**Ondrej Juhasz**  
Research Associate  
San Jose State University

## ABSTRACT

Linearized inflow models have been used to represent dynamic wake effects for control law development and flight dynamics simulation of conventional main rotor/tail rotor helicopters. For advanced rotorcraft configurations based on compound-coaxial and multi-rotor distributed propulsion, rotor-on-rotor and rotor-on-wing interactions lead to a breakdown of classical dynamic inflow theory. An approach for extracting low-order inflow models from comprehensive aerodynamic analyses has been investigated as part of continuing research and development toward an automated procedure for inflow/wake model identification. This paper describes the initial results for inflow model extraction from a full-span free wake analysis in hover, forward flight, and maneuvering flight conditions. Emphasis has been placed on the model structure formulation to yield identified inflow models that capture the critical dynamics associated with the rotor wake and induced velocity without being over-parameterized. Model structures previously reported in the literature do not capture all wake dynamics observed in a free wake model, some of which impact the coupled rotor-body response characteristics. Wake distortion effects due to tip path plane angular rate, off-rotor interference, and coaxial rotor interactions are examined herein.

## NOTATION

$C_T, C_L, C_M$	Aerodynamic thrust, roll moment, and pitch moment coefficients	$K_{R_1}, K_{R_2}$	Angular rate coefficients in second order inflow model
$C_{T_o}$	Trim thrust coefficient	$L, M$	Inflow static gain and apparent mass matrices
$C_{T_u}, C_{T_l}$	Coaxial upper and lower rotor thrust coefficient	$R$	Rotor radius
$F_s, G_s$	Second-order sine harmonic inflow state and control matrices	$T_u$	Coaxial rotor delay time (upper-to-lower)
$H_l^u, H_u^l$	Coaxial rotor inflow transfer functions	$v_h$	Trim rotor induced inflow, $v_h = \sqrt{C_{T_o}/2}$
$K_1, K_2$	Coaxial rotor inflow transfer function gains	$\gamma$	Rotor Lock number
$K_L$	Harmonic inflow due to aerodynamic loading	$\lambda_o, \lambda_c, \lambda_s$	Uniform and harmonic inflow states
$K_M$	Harmonic inflow near/far field coupling term	$\lambda_{ou}, \lambda_{ol}$	Coaxial upper and lower rotor uniform inflow
$K_R$	Harmonic inflow due to tip path plane rate	$\tilde{\lambda}_{ou}, \tilde{\lambda}_{ol}$	Coaxial inflow due to local loading effects
		$\lambda_{s_1}, \lambda_{s_2}$	Lateral harmonic inflow near and far field components
		$\sigma$	Rotor solidity
		$\tau_1, \tau_2$	Second order inflow model near and far field time constants
		$\omega_\beta$	Flap natural frequency
		$\Omega$	Rotor rotational speed

Presented at the AHS International 73rd Annual Forum & Technology Display, Fort Worth, Texas, USA, May 9-11, 2017. Copyright © 2017 by AHS International, Inc. All rights reserved. Approved for public release; distribution unlimited.

## INTRODUCTION

Modern helicopter flight control development, as well as flight dynamics simulation, use low-order state space models to represent rotor inflow dynamics. It is well known that rotor inflow dynamics affect the helicopter response and limit gains for high-bandwidth controllers (Ref. 1). Inflow models such as Pitt-Peters dynamic inflow (Ref. 2) and Peters-He finite state inflow (Ref. 3) have seen widespread application in conventional rotorcraft (main rotor/tail rotor) flight dynamics simulation and control law development. Modern rotorcraft, however, are transitioning to advanced concepts such as coaxial-compound and multi-rotor (distributed propulsion) tilt rotor/wing configurations. For these configurations, aerodynamic interactions between the primary lift-sharing components (e.g., rotor-on-rotor, rotor-on-wing, and rotor-on-airframe) can be significant, and these effects are not well represented by current state-space inflow models in their present form.

In contrast, physics-based free wake and computational fluid dynamics (CFD) models provide greater accuracy and flexibility in capturing interactional aerodynamic effects present in advanced rotorcraft configurations. In recent work (Ref. 4), a real-time free wake model was coupled with a nonlinear flight dynamics simulation for enhancing pilot-in-the-loop rotorcraft simulation. Free wake models, applied to high-resolution engineering analysis or real-time simulation, are not in a form for use with rotorcraft flight control design since the inflow and wake dynamics are embedded as internal (hidden) dynamic states. It is desirable to blend together these complementary methods (linearized state-space and nonlinear physics-based models) for flight control applications.

Previous work has been performed to formulate vortex wake models in a state-space structure (Refs. 5-7). In general, these approaches resulted in high-order models that were not easily applied in rotorcraft stability and control analysis. A more tractable approach for linearized inflow model extraction from high-fidelity aerodynamic analyses has been the focus of more recent work (Refs. 8, 9). In this work, a free wake model was used to determine an equivalent low-order inflow model that is suitable for helicopter stability and control analysis. The approach defined a model structure based on Pitt-Peters or Peters-He inflow models and used a single frequency analysis procedure or frequency sweep identification method to determine the model coefficients. This approach has been applied to an isolated rotor in hover, forward flight and maneuvering flight conditions, as well as to a coaxial rotor system.

An important aspect of the linear inflow model extraction process is identification of a suitable model structure that provides the sufficient degrees of freedom to capture relevant dynamics associated with the rotor wake but is not over-parameterized. Model over-parameterization will reduce the robustness of the extracted model. Model structure

formulation is examined in this paper that addresses maneuvering flight effects in hover, main rotor interference with the empennage/tail rotor, and multi-rotor interactions. It is shown that the conventional first-order state space model formulation associated with dynamic inflow theory is insufficient in capturing all dynamics observed in the free wake model. It is also shown that these dynamic effects can be represented by an augmented inflow state vector and corresponding state-space model structure. These dynamic effects introduced by the augmented state model structure are shown to impact rotor flapping and aircraft response, in particular for hover/low speed maneuvering flight.

This paper describes the initial research toward the development of an automated process for linearized inflow model extraction from high fidelity aerodynamic analyses. Linear model extraction has been performed using frequency-domain parameter identification techniques. The linearized inflow model extraction process, described in the following section, has used the Comprehensive Hierarchical Aeromechanics Rotorcraft Model (CHARM) free wake model (Refs. 4, 10-12) and CIPHER<sup>®</sup> frequency domain system identification method (Ref. 13). Following a description of the approach with application to a single rotor configuration, extensions of the basic approach are discussed to address wake distortion effects, rotor interference modeling, and application to coaxial rotor systems.

## LINEAR INFLOW MODEL EXTRACTION

The approach for linear inflow model extraction is described in this section. Following an overview of the CHARM model, the approach is applied to extract dynamic inflow coefficients for an isolated rotor. Results provide a benchmark of the methodology when compared with previous work (i.e., Refs. 8, 9), in addition to a foundation for investigation of model structure extensions.

### CHARM Model Overview

The Comprehensive Hierarchical Aeromechanics Rotorcraft Model (CHARM) is a comprehensive analysis with a free-vortex wake model that has been used for rotorcraft aerodynamics analysis applications. Description and validation of the CHARM model has been documented in the literature (Refs. 4, 10-12). An overview of several aspects of the model relevant to the present study is provided below.

The CHARM free wake model represents the full span vortex sheet from a rotor blade using a Constant Vorticity Contour (CVC) model. This approach represents both trailing and shed vorticity components that arise due to spanwise and azimuthal variations in the bound circulation. The CVC wake model is implemented using multiple equal and constant strength curved vortex elements released from the rotor blade (see Figure 1). This approach is computationally efficient while maintaining high fidelity for accurate predictions.

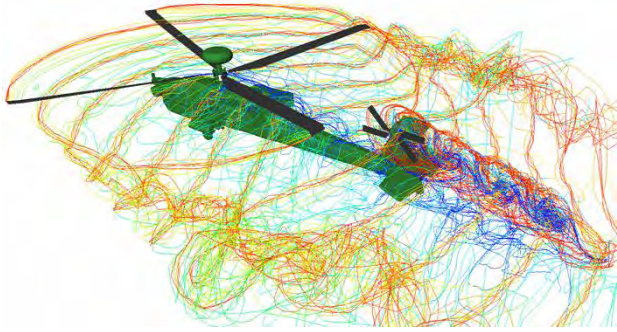


**Figure 1. CHARM CVC Wake Model for the AH-64 Main and Tail Rotors**

The wake-induced velocity field, which determines the free wake geometry and provides feedback to the rotorcraft aerodynamic loads, is determined from numerical summation for each vortex element based on the Biot-Savart law. The evaluation of the induced velocity can be done at control points located on the rotor blade/aerodynamic surface and away from the rotor. Off-rotor evaluations have been used to model rotor interference effects and rotor-on-rotor interactions for application to coaxial rotor systems. The Biot-Savart summation includes a vortex core model for each vortex element to prevent numerical singularities. The CVC model formulation does not preset the core model radius but instead determines the initial core size based on the blade circulation distribution. This approach concentrates vortex filaments in regions of high vorticity (e.g., near the blade tip) with smaller core radii. Downstream from the rotor blade, the full-span wake is consolidated into either a vortex pair (varying strength root and tip filaments) or a single tip vortex. This approach has been found to preserve solution accuracy while reducing computational overhead.

### Linearized Model Extraction Approach

Linearized inflow models were determined by using free wake analysis (CHARM) to generate inflow data due to prescribed inputs to the rotor. A linear model structure was prescribed, and model coefficients were determined using the CIFER<sup>®</sup> system identification method. Inflow data were obtained using frequency sweep and doublet/multi-step inputs. Frequency sweep and response data were used for model identification while doublet/multi-step response data were used for model time-domain verification. This approach conceptually was similar to Ref. 8 but applied different numerical methods. Note that the methods used in this phase of the research required intervention from the analyst, and future work will address automation of the procedure.

Rotor inflow data were determined by using CHARM with a specialized executive that was developed specifically for this application. In more typical applications, rotor blade airloads are provided to the free wake analysis, which are used to determine the blade circulation distribution and wake geometry in a time-accurate manner. The blade airloads can

be determined from quasi-steady sectional aerodynamics (strip theory) or unsteady vortex lattice methods, accounting for blade motion and flight dynamic response characteristics. For this application, the blade circulation distribution was prescribed in a manner to produce a (nearly) pure thrust or aerodynamic moment response on the rotor, and correspondingly little to no correlation between inputs. The rotor system also was approximated as rigid to remove flap (and lag/torsion) effects on the inflow response.

Instantaneous snapshots of the wake geometry modeled by CHARM to generate inflow data for linear model extraction are shown in Figure 2. This approach for inflow source data generation was found to work well in producing approximately uncoupled thrust and aerodynamic moments, which improved the ability to estimate frequency responses without requiring special considerations for multiple inputs.

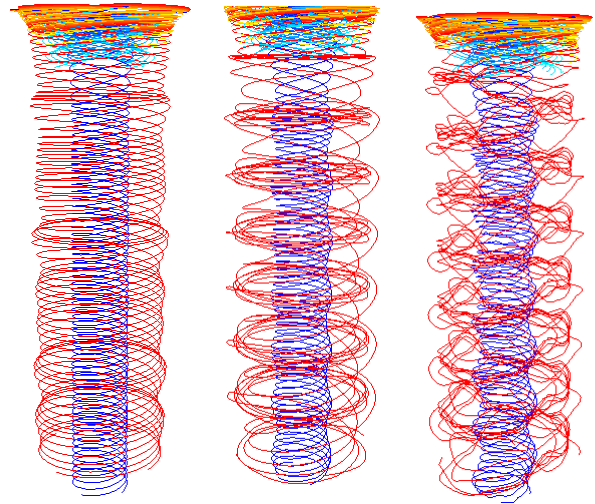


**Figure 2. Free Wake Geometry Snapshots for Trim (left), Thrust (center) and Pitch Moment Perturbation (right)**

Rotor inflow states were determined by evaluation of the wake-induced velocity at aerodynamic control points along each blade as the blade circulation distribution was prescribed as a function of time. At each time step, the induced velocity field was projected onto radial/harmonic basis functions. Several numerical integration methods also were investigated for performing the inflow state projection. For the results presented in this paper, a three-state inflow expansion was used ( $\lambda = \lambda_o + \lambda_c x \cos \psi + \lambda_s x \sin \psi$ ) in conjunction with a swept area weighted integration method to determine the inflow coefficients.

Inflow data were generated for frequency response estimation in hover and forward flight conditions. Unless otherwise noted, results presented in the paper were obtained for a generic four-bladed rotor system with dimensions representative of a UH-60 main rotor. Forward flight conditions examined in this investigation were 20, 40, 80, and

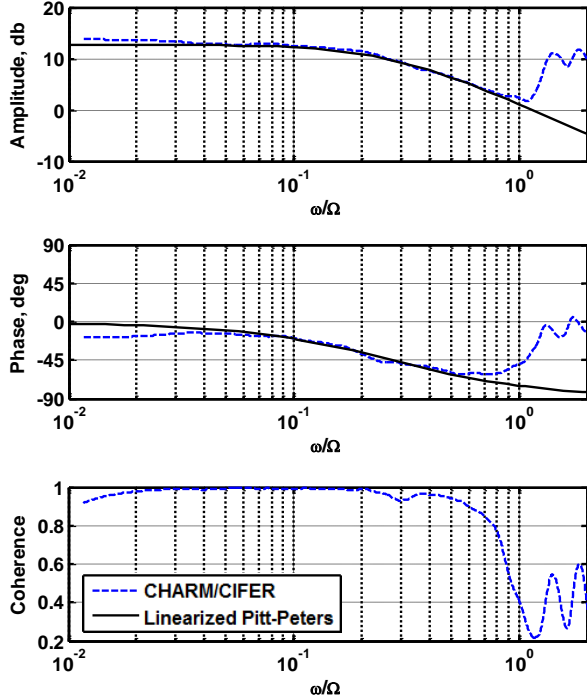


Figure 3. CHARM  $\lambda_o/C_T$  Frequency Sweep, Hover

120 knots (advance ratio of 0.047, 0.093, 0.19, and 0.28) with shaft angle of attack determined from a full aircraft trim solution. The trim thrust coefficient was 0.007, and shaft angle of attack was approximately -5 degrees (nose down) for the 120-kt case. Inflow response data were obtained due to thrust / aerodynamic moment perturbations and tip path plane angular rate inputs.

Time-sampled rotor inflow input/output data were imported into CIFER<sup>®</sup> for analysis and model identification. Frequency sweep data were obtained for approximately 100 seconds. The duration and sampling rate of these data permitted definition of four different window sizes (20-sec, 10-sec, 5-sec, 2-sec) that were merged into a single composite window for each frequency response input-output pair. Representative estimated frequency responses are illustrated in Figure 3 and Figure 4 for the hover case. Note that the frequency axis in Figure 3 and Figure 4 has been normalized by the rotor rotational rate. For comparison, the corresponding responses based on linearized Pitt-Peters dynamic inflow theory also are plotted and are similar to the estimated responses using CHARM.

The results in Figure 3 and Figure 4 show that in hover the extracted inflow responses are low-order and linear for  $\omega/\Omega$  less than 0.5, which corresponds to the maximum excitation frequency. Furthermore, the collective axis response very nearly matches the Pitt-Peters model over a broad frequency range. The lateral inflow response primarily differs by a gain offset.

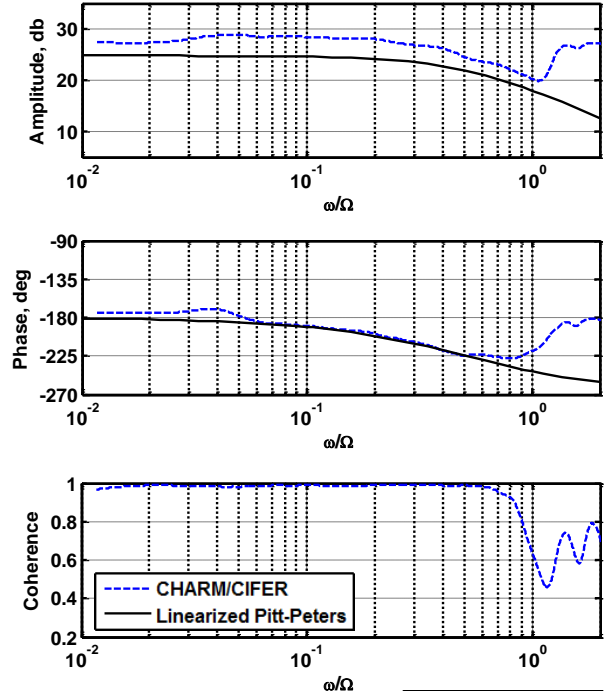


Figure 4. CHARM  $\lambda_s/C_L$  Frequency Sweep, Hover

### Three State Inflow Model Identification

Extraction of a linearized inflow model was performed using frequency-domain parameter identification and required a suitable model structure to be specified. For the hover/forward flight response data, a conventional three-state Pitt-Peters dynamic inflow model structure was used, i.e.,

$$M\dot{v} + L^{-1}v = F \quad (1)$$

with  $v = [\lambda_o \quad \lambda_s \quad \lambda_c]^T$ ,  $F = [C_T \quad C_L \quad C_M]^T$ , and

$$M = \begin{bmatrix} M_{11} & 0 & 0 \\ 0 & M_{22} & 0 \\ 0 & 0 & M_{33} \end{bmatrix}$$

$$L = \begin{bmatrix} L_{11} & 0 & L_{13} \\ 0 & L_{22} & 0 \\ L_{31} & 0 & L_{33} \end{bmatrix}$$

The “off-axis” terms in the  $L$ -matrix representing coupling between the uniform/cosine harmonic and sine harmonic components, which are identically zero based on the theoretical formulation given by Pitt and Peters (Ref. 2), are non-zero but generally small for the free wake model. Linear model extraction has been performed using a full  $L$ -matrix structure, but these results are not presented in this paper.

For model identification, it was more convenient to re-write Eq. (1) as:

$$LM \dot{v} + v = LF \quad (2)$$

The matrix ( $LM$ ) can be viewed as an effective “time constant” matrix (Ref. 14). In hover, the time constant matrix will be diagonal with equal values for the sine and cosine inflow harmonics due to axial symmetry. Due to the presence of the ( $L_{13}$ ,  $L_{31}$ ) terms, this matrix is not diagonal nor symmetric in forward flight.

A summary of the identified model cost functions is given in Table 1 through Table 4 for hover, 40, 80, and 120 knots conditions. For the 20-kt case, the coherence for all frequency responses was insufficient for model identification. This flight condition corresponds to the transition between low-and high-speed, and longer input-output data records may be required for model identification during transition. Initially, only the inflow apparent mass and static gain coefficients were freed in the model structure, and it was found that the model structure did not adequately match the frequency response data from CHARM. In particular, this discrepancy was more pronounced in the off-diagonal responses ( $\lambda_o/C_M$ ,  $\lambda_c/C_T$ ) for low to moderate forward speeds. Time delay parameters were included in the model structure to improve the model fit to the CHARM data, as summarized by the final identified cost functions in Table 1 through Table 4. For thrust inputs, separate time delays were applied to the uniform and cosine harmonic inflow responses, which was required for the 40-kt case. The average cost for the identified models with time delays was on the order of 100 or less indicating a good fit.

Identified inflow model parameters are summarized in Table 5, which includes estimates of parameter uncertainties (i.e., CIFER<sup>®</sup> Cramer-Rao bounds). Tabulated time delay parameters have units of milliseconds. The inflow mass matrix elements were identified but then normalized by the rotor speed  $\Omega = 27$  rad/sec to permit comparison with theory and other results in the literature. The extracted linear inflow model coefficients are compared to theoretical values for Pitt-Peters dynamic inflow theory in Figure 5. The theoretical and identified model coefficients have similar magnitudes and trends with forward speed, although the identified harmonic inflow gains due to aerodynamic moments are larger than theory. Similar results can be derived from Ref. 9, which are plotted in Figure 5 for comparison. The plotted results from Ref. 9 are derived based on the “generalized state-space” model with rotor thrust coefficient and angle of attack schedule matching the current analysis. Note that this generalized state space model provides functional forms for the inverse inflow gain matrix coefficients, which have been inverted to compare with the model given in this paper.

For the inflow mass matrix, dynamic inflow theory predicts

$$M_{11} = \frac{8}{3\pi} = 0.849$$

$$M_{22,33} = -\frac{16}{45\pi} = -0.113$$

The extracted linear inflow model resulted in coefficients with similar magnitude but that vary with forward speed. Axial symmetry of the mass matrix was maintained in forward flight as indicated by the similar identified values for the  $M_{22}$  and  $M_{33}$  terms in Table 5. This result was not observed when the input time delays were not included in the identified model structure.

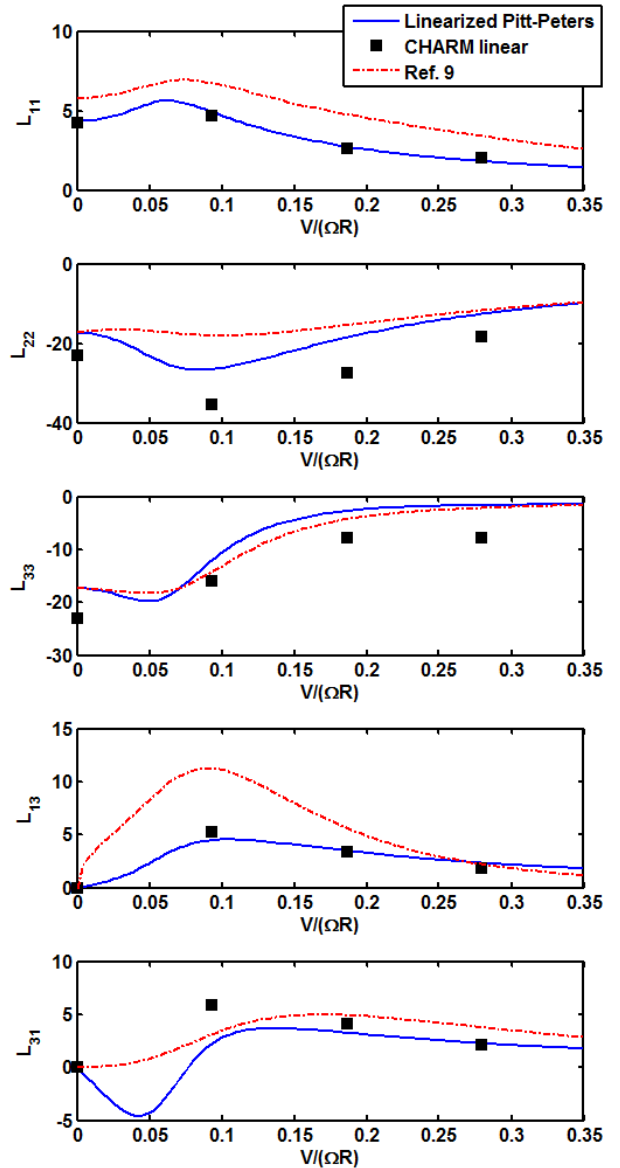


Figure 5. Comparison of Identified L-matrix with Theory

**Table 1. Identified Model Cost Function, Hover**

Response	Final Cost
$\lambda_o/C_T$	14.5
$\lambda_s/C_L$	43.1
Ave. cost	28.8

**Table 3. Identified Model Cost Function, V=80kts**

Response	Final Cost	Final Cost with Delay
$\lambda_o/C_T$	72.4	87.7
$\lambda_s/C_L$	136.8	50.3
$\lambda_c/C_M$	149.5	149.4
$\lambda_o/C_M$	423.4	108.2
$\lambda_c/C_T$	390.2	130.2
Ave. cost	234.5	105.1

**Table 2. Identified Model Cost Function, V=40kts**

Response	Final Cost	Final Cost with Delay
$\lambda_o/C_T$	167.5	4.9
$\lambda_s/C_L$	122.3	17.6
$\lambda_c/C_M$	363.9	94.9
$\lambda_o/C_M$	523.6	39.8
$\lambda_c/C_T$	5776.2	98.9
Ave. cost	1390.7	51.2

**Table 4. Identified Model Cost Function, V=120kts**

Response	Final Cost	Final Cost with Delay
$\lambda_o/C_T$	47.5	75.4
$\lambda_s/C_L$	66.4	22.3
$\lambda_c/C_M$	98.6	119.9
$\lambda_o/C_M$	382.8	104.1
$\lambda_c/C_T$	125.7	125.8
Ave. cost	144.2	89.5

**Table 5. Identified Linearized Inflow Model Parameters**

Parameter	Hover	V = 40 kts	V = 80 kts	V = 120 kts
$M_{11}$	0.689 (8.4%)	1.40 (5.2%)	1.51 (6.0%)	1.52 (6.9%)
$M_{22}$	-0.0675 (11.7%)	-0.119 (9.7%)	-0.162 (8.2%)	-0.168 (10.5%)
$M_{33}$	-0.0675 <sup>†</sup>	-0.125 (10.8%)	-0.182 (9.4%)	-0.164 (13.1%)
$L_{11}$	4.20 (4.3%)	4.66 (4.6%)	2.59 (4.2%)	2.04 (4.2%)
$L_{22}$	-23.0 (4.0%)	-35.3 (4.7%)	-27.6 (4.7%)	-18.4 (4.6%)
$L_{33}$	-23.0 <sup>†</sup>	-16.0 (4.7%)	-7.88 (4.6%)	-7.87 (4.1%)
$L_{13}$	0 <sup>†</sup>	5.21 (4.1%)	3.35 (3.9%)	1.82 (4.0%)
$L_{31}$	0 <sup>†</sup>	5.87 (4.1%)	4.08 (3.8%)	2.15 (3.9%)
$\tau_{C_T-\lambda_o}$	0 <sup>†</sup>	33.4 (23.8%)	79.6 (8.4%)	55.5 (10.5%)
$\tau_{C_L}$	0 <sup>†</sup>	59.8 (16.4%)	45.5 (15.8%)	35.0 (22.5%)
$\tau_{C_M}$	0 <sup>†</sup>	68.4 (12.2%)	66.4 (8.9%)	55.8 (11.1%)
$\tau_{C_T-\lambda_c}$	0 <sup>†</sup>	342 (3.3%)	79.6 <sup>†</sup>	55.5 <sup>†</sup>

<sup>†</sup> Parameter fixed or constrained during identification process

These results indicate that the linear model extraction can produce consistent results with theory and other analysis. Note that the large identified time delay for the 40-kt case (342 msec) suggests that the dynamic inflow model structure may be inadequate for low speed transition. Further investigation of the low speed transition regime is required. The following section provides additional insight when tip path plane motion effects are also considered in the model structure.

## WAKE DISTORTION EFFECTS

Rotor tip path plane angular rate is known to result in inflow variations that occur due to changes in the wake structure (i.e., wake distortion effects). Previously these effects have been included in state-space inflow models as an additive effect, e.g.,  $\Delta\lambda_c = K_R(q/\Omega)$  (Ref. 15). The linear inflow model extraction approach has been applied to identify a model for wake distortion effects due to rotor angular rate in hover. It has been found that an expanded inflow model structure is required to capture the relevant wake dynamics.

### CHARM Inflow Response

Roll and pitch rate inputs were applied to CHARM to generate data for inflow component frequency responses estimation. The angular rate inputs were applied about the tip path plane, which include both body angular rate ( $p/\Omega$ ,  $q/\Omega$ ) and harmonic flapping rates ( $\dot{a}_1/\Omega$ ,  $\dot{b}_1/\Omega$ ) in hover. In forward flight, a distinction must be made with respect to the axis (e.g., wind versus body axis) about which the pitch rate is applied, which affects the frequency response estimation procedure. This distinction typically is not required for roll rate inputs except for low-speed, large-sideslip flight conditions (e.g., sideward flight). These effects should be noted, although results presented herein focus on the hover case where axial symmetry and the interchange of body and tip path plane rates can be applied.

The lateral harmonic inflow frequency response due to roll rate is shown in Figure 6. Due to axial symmetry in hover, the longitudinal harmonic inflow response due to pitch rate is identical. Also shown in Figure 6 is a theoretical model provided by Curtiss (Ref. 16). This model considered the dynamics of the wake curvature due to angular rate following a step change in rate based on an indicial response analysis. This effect also was examined in Ref. 17. The Curtiss model can be represented as a first-order system. The time constant associated with the wake curvature dynamics tends to be much slower than the time constant associated with aerodynamic loading inputs, which is captured by the Pitt-Peters dynamic inflow model.

Comparison between the Curtiss wake distortion model and frequency responses extracted from CHARM in Figure 6 suggests that higher-order dynamics are present in the inflow/wake response. A similar observation can be made through

examination of Figure 4. Since the coherence is near unity in the frequency range where the free wake model deviates from theory, the discrepancy cannot be attributed to inaccuracies in the CHARM frequency response estimation or nonlinearities but rather represents the presence of unmodeled dynamics. Thus, an alternative inflow model structure has been investigated to capture the response predicted by free wake analysis.

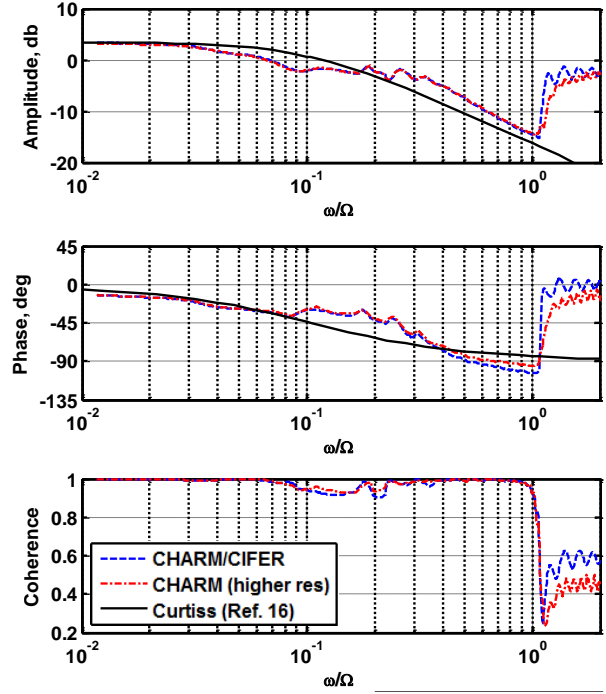


Figure 6. CHARM  $\lambda_s/(p/\Omega)$  Frequency Sweep, Hover

### Second Order Inflow Model Structure

Given the inability of the first-order theoretical models to capture the observed frequency response characteristics from free wake analysis, an expanded model structure was investigated for representing the harmonic inflow dynamics due to aerodynamic loading and angular rate wake distortion effects. The model is presented here in state-space form compatible with CIFER<sup>®</sup> frequency-domain identification.

The expanded inflow model structure reflects the observation that there are two characteristic time scales in the dynamic response: (1) a fast inflow mode that can be associated with changes in rotor loading and (2) a slow inflow mode associated with far-field wake distortion effects. Thus, a second-order model structure is used:

$$\begin{aligned} \dot{\Lambda} &= F_s \Lambda + G_s \Phi \\ \lambda_s &= [1 \quad 1] \Lambda \end{aligned} \quad (3)$$

with state vector defined as  $\Lambda \equiv [\lambda_{s_1} \ \lambda_{s_2}]^T$ . The input vector  $\Phi \equiv [C_L \ p/\Omega]$  includes both aerodynamic loading and angular rate components. Due to axial symmetry in hover, the above model structure applies for both sine and cosine harmonic inflow components. A more general model structure is necessary for forward flight conditions.

A loose physical interpretation of the above model structure is that the harmonic inflow response can be represented by the superposition of two components corresponding to the slow and fast inflow/wake modes. The state and input matrices ( $F_s$ ,  $G_s$ ) represent these dynamic characteristics, as well as coupling between the inflow states associated with short-term and long-term responses. Fully populated state and input matrices will result in eight free parameters. Based on the frequency responses in Figure 4 and Figure 6 estimated from free wake analysis, the expected number of unique free parameters is six, e.g., two poles, two zeros, and two gains associated with the  $\lambda_s/C_L$  and  $\lambda_s/(p/\Omega)$  transfer functions. Identification of model parameters and sensitivities using fully-populated  $F_s$  and  $G_s$  confirmed this result in which large uncertainties and correlated parameters were observed when more than six free parameters were included in the model structure.

Note that it was also found in Ref. 8 that extraction of linear inflow models from free wake analysis produced second-order response behavior for the harmonic inflow resulting from aerodynamic moments. Therefore, results presented in this paper are qualitatively consistent with Ref. 8. In contrast, Ref. 8 demonstrated that a rigid wake model resulted in the first-order behavior more commonly associated with dynamic inflow theory. It can be concluded that the observed higher-order behavior arises due to the far field (free) wake dynamics.

## Identification Results

Parameters for the expanded second-order inflow model were determined using a model structure with selected matrix elements fixed to eliminate parameter correlation. The choice of which parameters to hold at fixed values was determined iteratively and considered the magnitude of the identified parameters relative to theoretical values as appropriate. Identified parameter values and CIPHER<sup>®</sup> Cramer-Rao bounds are summarized in Table 6 representing the model structure that best satisfied this criterion.

Identified models for the  $\lambda_s/C_L$  and  $\lambda_s/(p/\Omega)$  responses are compared with theory in Figure 7 and Figure 8, respectively, in addition to the extracted response from the CHARM/CIPHER analysis. In Figure 7, two identified models are shown, one derived from the Pitt-Peters model structure (Eq. 1) and one based on Eq. (3). The identified Pitt-Peters model, while showing improvement as compared to the theoretical model, does not capture the second-order nature of the response. The identified second-order model captures the

additional lead introduced due to coupling of the near-wake and far-wake dynamics.

Figure 8 compares the harmonic inflow response due to roll rate for the identified second-order inflow model with theory from Ref. 15 and free wake analysis. The theory from Ref. 15 is equivalent to Pitt-Peters dynamic inflow theory with an added term proportional to the rotor tip path plane angular rate to represent wake distortion effects. All models recover the same steady state behavior, but the free wake analysis and identified model deviate from previous theory (Ref. 15) for non-dimensional frequencies greater than about 0.05, which corresponds to 1-2 rad/sec for the example rotor. Examination of both Figure 7 and Figure 8 indicates that the phase response for the identified second order model structure does not capture the free wake analysis for  $\omega/\Omega$  greater than approximately 0.3 (8 rad/sec for the example rotor). For the inflow response due to aerodynamic moment, the identified model over-predicts the phase lag, while phase is under-predicted for inflow response due to angular rate. The reason of this discrepancy has not been identified at this time. Since the discrepancy occurs within the frequency range of interest for flight control loop closures and piloted handling qualities, additional investigation may be warranted.

**Table 6. Summary of Second Order Inflow Model Identification Results**

Parameter	Value
$F_{11}$	-10.4 (10.1%)
$F_{12}$	0 <sup>†</sup>
$F_{21}$	-0.562 (23.0%)
$F_{22}$	-1.31 (20.3%)
$G_{11}$	-300 (8.3%)
$G_{12}$	5.68 (12.7%)
$G_{21}$	0 <sup>†</sup>
$G_{22}$	1.32 (18.8%)
Ave. cost	27.8

<sup>†</sup> Parameter fixed during identification process

## Physical Interpretation of Identified Model

A physical interpretation of the expanded model structure and identified parameters is provided. Recall that for the identified model structure it was postulated that the harmonic inflow can be separated into two parts representing the near-field ( $\lambda_{s_1}$ ) and far-field ( $\lambda_{s_2}$ ) effects, each of which contribute to the total inflow through the rotor ( $\lambda_s = \lambda_{s_1} + \lambda_{s_2}$ ). Normalizing the time derivatives by  $\Omega$  and rearranging yields the following model structure:

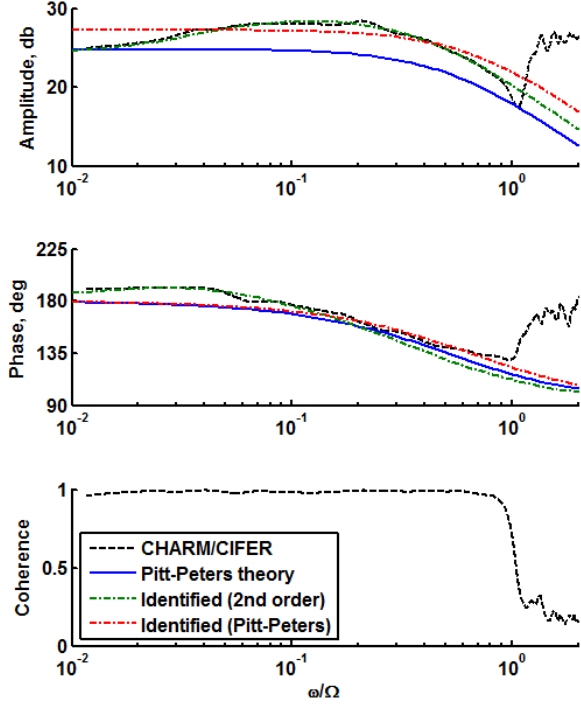


Figure 7. Comparison of Identified  $\lambda_s/C_L$  Models with Theory and CHARM/CIFER Extracted Response, Hover

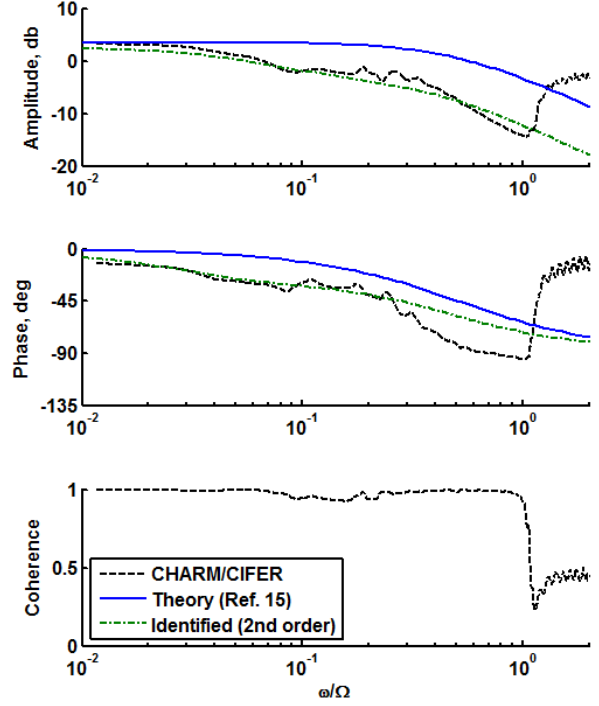


Figure 8. Comparison of Identified  $\lambda_s/(p/\Omega)$  Model with Theory and CHARM/CIFER Extracted Response, Hover

$$\begin{aligned} \overbrace{\tau_1 \dot{\lambda}_{s_1} + \lambda_{s_1}} &= K_L C_L + K_{R_1} \left(\frac{p}{\Omega}\right) \\ \tau_2 \dot{\lambda}_{s_2} + \lambda_{s_2} &= -K_M \lambda_{s_1} + K_{R_2} \left(\frac{p}{\Omega}\right) \end{aligned} \quad (4)$$

Values and physical interpretations for the model parameters are given in Table 7. The bracketed part of the first equation represents the near-field harmonic inflow variation due to

aerodynamic loading and is equivalent to the linearized Pitt-Peters dynamic inflow model. The effect of wake distortion due to angular rate for the near-field primarily is governed by the relative change in vertical spacing of the successive turns of the wake structure, an effect that was modeled in Ref. 18. Theoretically, the parameter value representing this effect has been predicted using simple vortex analysis to be 0.5 (Ref. 19), which is close to the identified value of 0.55.

Table 7. Second Order Inflow Model Parameters and Physical Interpretations

Parameter	Description	Theory	Identified
$K_L$	Inflow static gain due to aerodynamic loading (Pitt-Peters)	-17.3	-28.8
$\tau_1$	Near-field inflow time constant (Pitt-Peters)	1.96	2.60
$\tau_2$	Far-field inflow time constant (Ref. 16)	13.8	20.6
$K_{R_1}$	Near-field wake distortion effect (Refs. 18, 19)	0.5	0.55
$K_{R_2}$	Far-field wake distortion effect ( $K_R = K_{R_1} + K_{R_2}$ )	1.0	1.01
$K_M$	Near-field/far-field coupling term	N/A	0.43

For the far-field contribution, the time constant ( $\tau_2$ ) was predicted by Curtiss to be  $0.8/v_h$ , where  $v_h$  is the average uniform induced inflow through the rotor (Ref. 16). The far-field wake distortion effect arises due to wake curvature, and theoretically the combined effect of wake distortion should yield the value predicted by vortex tube analysis in the steady-state limit (i.e.,  $K_R = K_{R_1} + K_{R_2} = 1.5$ ). The last parameter in the model ( $K_M$ ) represents the effect of the harmonic induced velocity on the wake in the far field. This parameter has not been determined from theory, although Curtiss notes in Ref. 16 that “the effect of the distorted wake [due to the induced inflow gradient] is reduced by a factor equal to 0.4”. While the theoretical and identified values do not exactly match (in particular the time constants), the physical interpretation of the model and closeness of many parameter values with theory provide credibility to the identified model structure.

## Rotor Flapping Response

The identified inflow model was integrated with a separate model for the flap response of an isolated rotor and compared with response predictions using CHARM. This additional verification step compared the linearized flap/inflow model with results generated from nonlinear aerodynamics and free wake analysis. The cyclic flapping response due to cyclic pitch and pitch/roll rate in hover has been derived in several references (e.g., Ref. 20). The inflow dynamics are coupled through the aerodynamic moments on the rotor. In the rotor inflow response, the effect of wake distortion requires that the roll rate (and pitch rate) include terms proportional to the cyclic flapping rate. These terms arise since the wake dynamics depend on the motion of the tip path plane.

Calculations of the flap response of an isolated rotor due to cyclic pitch and hub rate inputs have been performed to illustrate the effect of the inflow model. Results shown herein correspond to a rotor representative of an H-60. Model parameters are tabulated in Table 8.

First, the effect of the inflow model on the rotor flap response is considered. The flap response due to a step change in longitudinal cyclic pitch is shown in Figure 9 illustrating the effect of the inflow model. It can be seen that the longitudinal flap response for the linearized Pitt-Peters and CHARM linear extracted models are similar, where the extracted model structure corresponds to Eq. (3) with flapping rate terms included with the angular rate. The curve in Figure 9 based on the model from Ref. 15 corresponds to the linearized Pitt-Peters model with an additive term proportional to the tip path plane rate, i.e.,  $\Delta\lambda_s = K_R(p + \dot{b}_1)/\Omega$  with  $K_R = 1.5$ , representing the effect of wake distortion due to tip path plane motion. When included with the flap dynamics in this form, the progressing flap mode is destabilized. With the CHARM-extracted linear model, the progressing flap mode is damped, which results from the slow far-field wake dynamics and attenuates the destabilizing effect of wake distortion.

**Table 8. Isolated Rotor Flap Response Study Parameters**

Parameter	Value	Description
$R$	26.83	Rotor radius, ft
$\Omega$	27	Rotor speed, rad/sec
$\omega_\beta$	1.035	Flap frequency
$\gamma$	8.1	Lock number
$\sigma$	0.0821	Rotor solidity
$C_{T_0}$	0.0067	Trim thrust coefficient

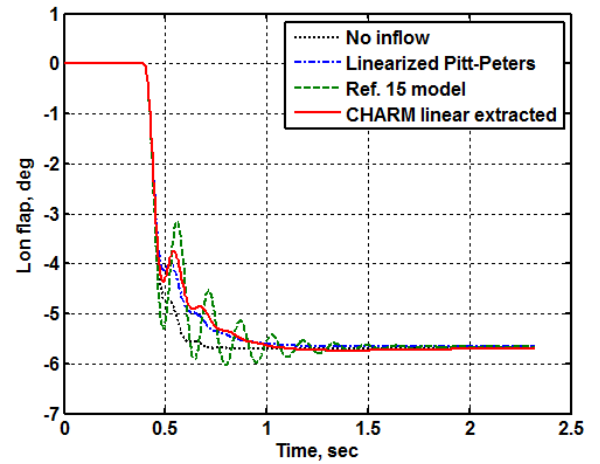


**Figure 9. Effect of Inflow Model on Flap Response due to Longitudinal Cyclic Pitch ( $B_{1_s}$ ) Input**

The rotor flap response with the CHARM linear extracted inflow model has been compared with the flap response predicted using the CHARM stand-alone analysis, which also models blade motion and aerodynamic loads. Results for the flap response due to a 2-deg lateral cyclic step input is shown in Figure 10, and the response due to a 5 deg/sec step roll rate input is shown in Figure 11. The CHARM analysis response was determined by trimming to a steady thrust coefficient of 0.0067, holding this condition for 10 seconds to allow wake unsteadiness to settle, and then applying the input and transient solution. For reference, results with the linearized Pitt-Peters model are also shown in Figure 10 and Figure 11. The flap response with the CHARM-extracted inflow model compares favorably with the stand-alone analysis and captures many key features of the response. In particular for the flap response due to angular rate, where both a small overshoot in the on-axis flap response, as well as the correct sign and magnitude of the off-axis flap response, are captured with the CHARM-extracted linear model. Thus, the extracted model captures the critical dynamics associated with a nonlinear free wake analysis.

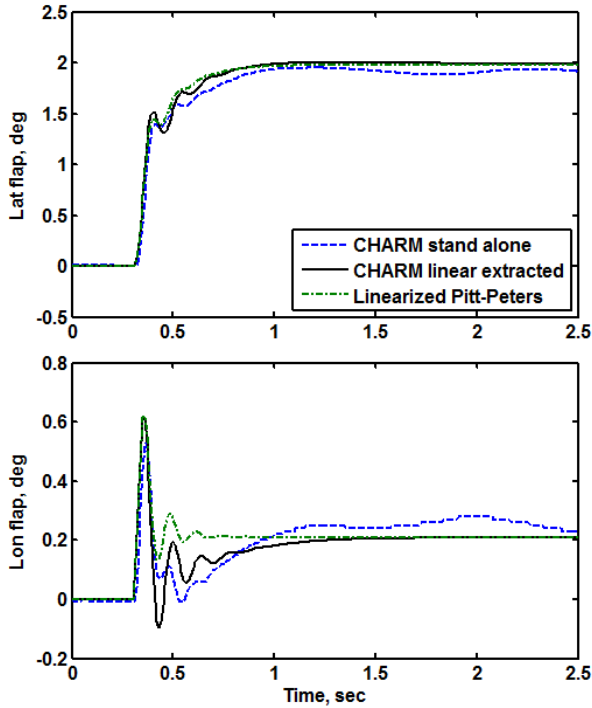


Figure 10. Comparison of Linearized Model Flap Response due to Lateral Cyclic Pitch ( $A_{1s}$ ) with Full CHARM Analysis

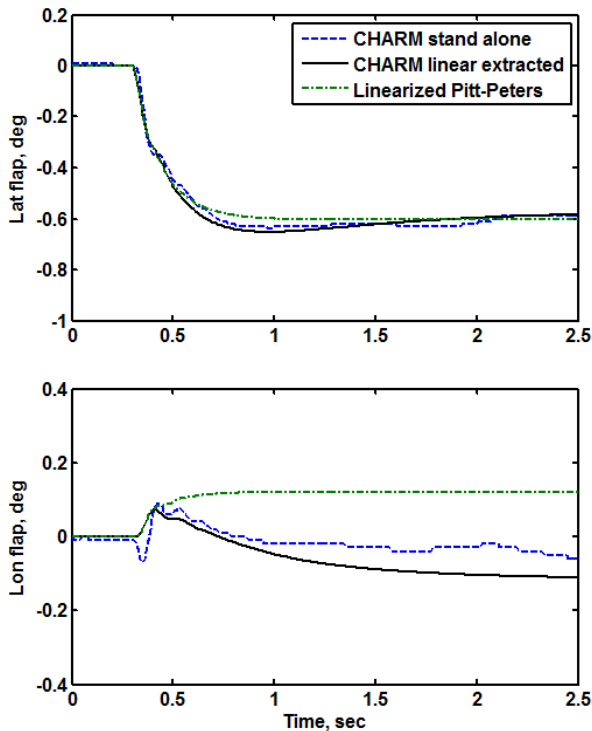


Figure 11. Comparison of Linearized Model Flap Response due to Roll Rate with Full CHARM Analysis

Note that the idealized step input used to generate the responses shown in Figure 9 through Figure 11 excites higher frequency modes more so than a typical input applied by a pilot. Thus, these results tend to provide more excitation to the progressing flap mode than might be encountered with typical pilot inputs in flight dynamics simulation or handling qualities activities. Capturing the second-order nature of the harmonic inflow response for the coupled flapping and inflow/wake physics will be more important when assessing high bandwidth flight control design performance.

## MAIN ROTOR INTERFERENCE MODELING

The rotor induced velocity field affects aerodynamic loads generated by the fuselage and other lifting surfaces (i.e., rotor interference effects at the empennage), which can influence trim and dynamic response characteristics. In rotorcraft flight dynamics simulation, rotor interference typically is modeled as a nonlinear function (look-up table) that depends on the rotor velocity state (e.g., advance ratio, angle of attack) and scales with the mean inflow through the rotor. Non-uniformity of the induced velocity field, due to the asymmetry between advancing and retreating sides in forward flight, provides an additional source of coupling between longitudinal and lateral motions. Non-uniform interference also has been shown to affect helicopter stability and control (Ref. 21). In addition, the velocity field induced by the rotor wake at aerodynamic surfaces away from the rotor introduces dynamics that can be represented by a time delay. This delay reflects the transit time for an aerodynamic perturbation at the rotor to propagate to the empennage surface.

The procedure used to extract linearized models for the rotor inflow response also has been applied to induced velocity effects away from the rotor. This approach was applied for developing a model for main rotor interference at the empennage of a conventional helicopter configuration. A more general application can include modeling interactions between rotating and non-rotating aerodynamic components. Note that the approach outlined in this section is used to represent the dynamics of the rotor-empennage interference and should be combined with a conventional nonlinear look-up table to account for non-uniform interference effects.

### CHARM Interference Data

The CHARM model was used to generate rotor wake induced velocity data at evaluation points located off the rotor plane, and these data were used to extract frequency responses and corresponding parametric models. The induced velocity at fixed evaluations points was determined due to rotor loading and tip path plane motion (frequency sweep) inputs. Several evaluation points were located beneath the rotor along the aircraft centerline (see Figure 12) to investigate the effect of spatial position. Note that Point 5 in Figure 12 corresponds to the center of the horizontal tail (stabilator) for the H-60. In

addition, the induced velocity was determined at evaluation points located along the horizontal stabilator to investigate the effect of induced velocity non-uniformity.

Frequency sweep source data from CHARM for an 80-knot level flight condition were analyzed, and representative results are shown in Figure 13 and Figure 14. The frequency responses represent the downward component of the interference velocity (downwash) at a given point or averaged across the horizontal tail (for Figure 13) due to the average inflow through the rotor. For the low frequency range, the interference state response at the empennage due to rotor uniform inflow perturbation has characteristics of a gain plus delay, which is expected and is a standard wing-on-tail and rotor-on-tail interference modeling method. For higher frequency excitation, additional dynamic characteristics are apparent and have characteristics of a “structural” pole-zero pair. For evaluation point locations positioned closer to the rotor (Points 2 and 3 in Figure 14), the nature of the dynamic response becomes less clear, although the drop in coherence indicates that other wake dynamics unrelated to the input are present.

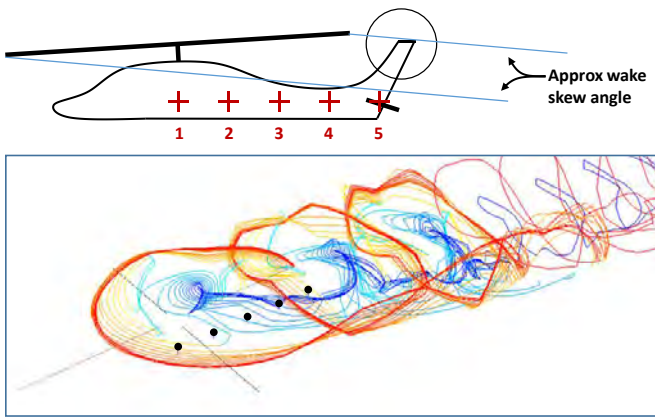


**Figure 12. Representative Off-rotor Evaluation Point Locations for Linearized Interference Model Extraction**

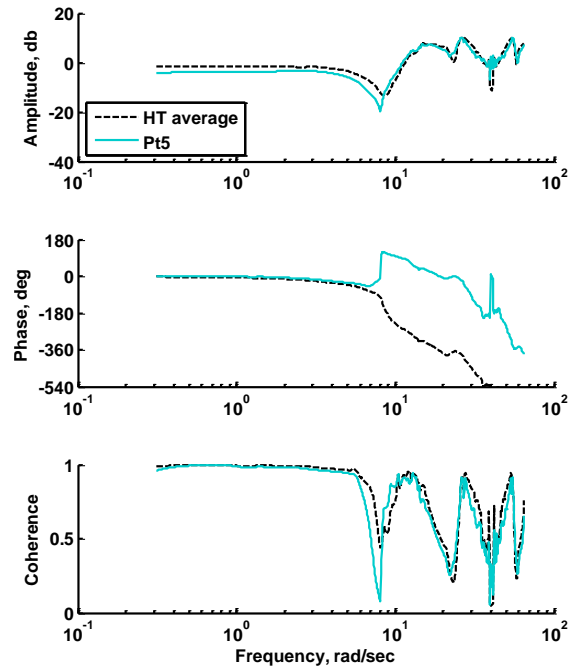


**Figure 13. Comparison of Single Point and Averaged Interference Frequency Responses**

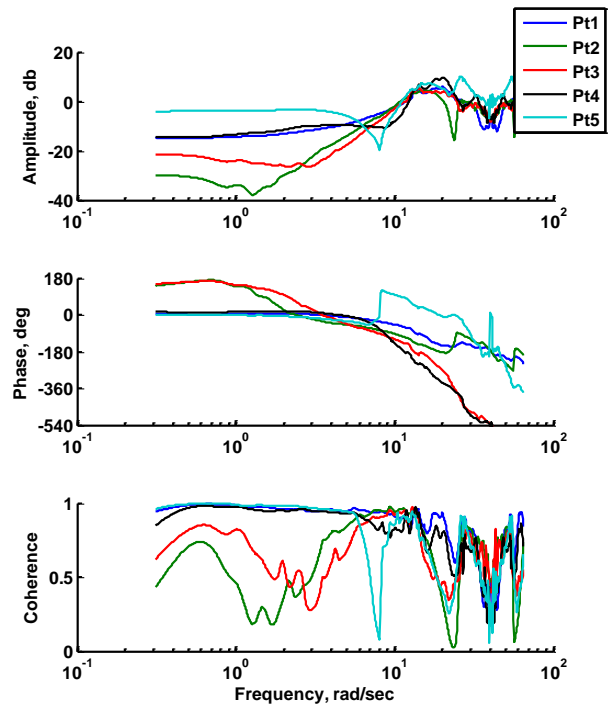


**Figure 14. CHARM Interference Component Frequency Response due to Rotor Uniform Velocity Perturbation**

## Linearized Interference Model Extraction

Extraction of a linearized interference model was performed using a model structure that accounts for the gain/delay between the off-rotor interference state and main rotor inflow. The model structure was sufficient to capture response characteristics over the frequency range of interest in piloted handling qualities (1-10 rad/sec). This model structure also included a provision to represent the pole-zero behavior near 8 rad/sec. The specific details for the model structure derivation are lengthy but follow standard practices for frequency-domain parameter identification (Ref. 13). Comparison of the identified model and CHARM in the time domain is shown in Figure 15. This model was coupled with a nonlinear flight dynamics simulation. It was found to provide on-axis response consistent with the baseline nonlinear Pitt-Peters inflow model and with the CHARM wake module integrated with the rotor blade element model (Ref. 4). Note that dynamics associated with the interference states are expected to have lesser impact on rotorcraft flight dynamics than the rotor inflow dynamics; this will be investigated more in future work.

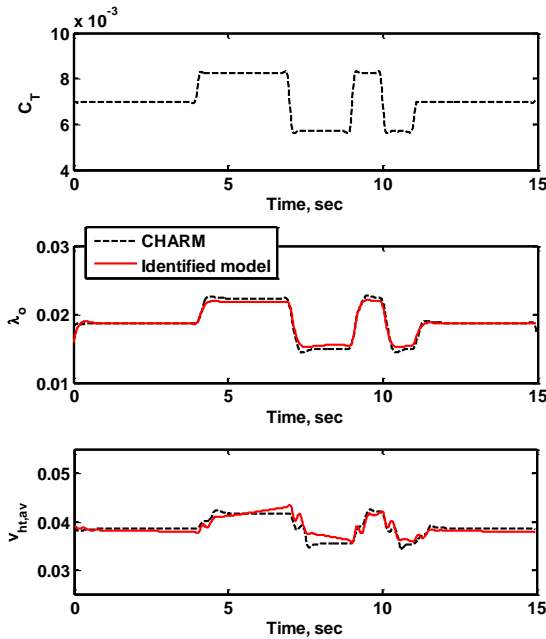


Figure 15. Inflow / Interference Model Verification for  $C_T$  Input,  $V = 80$  kts

## COAXIAL ROTOR SYSTEM MODELING

A primary motivation for linear inflow model extraction from higher fidelity aerodynamic analyses is in the application to advanced rotorcraft configurations with multiple rotating and fixed lifting components in close proximity. For these rotorcraft configurations, strong interactions between the aerodynamic loads and wakes can be expected, which should be reflected in the low-order models used for flight dynamics

analysis and control system development. Current theoretical models do not account for these interactions between multiple rotors and/or fixed lifting surfaces. To investigate application to advanced rotorcraft configurations, the current approach was used to extract a linear inflow model for an isolated coaxial rotor system in hover.

## CHARM Coaxial Rotor Model

Demonstration of the CHARM/CIFER methodology was performed using a representative coaxial rotor system based on two counter-rotating four-bladed rotors. The blade geometry was based on dimensions and sectional characteristics of an H-60 rotor. The vertical spacing between rotors was approximately 5 feet ( $h/2R = 0.1$ ). The combined trim thrust coefficient for the rotor system was approximately 0.0067 with equal thrust sharing for both upper and lower rotors. As with the single rotor cases discussed previously in this paper, frequency sweep inputs were applied separately to the upper and lower rotors to generate inflow data for linearized model extraction. Inflow responses were determined for the upper and lower rotors, which provided source data for model identification.

Frequency responses are shown in Figure 16 that illustrate the upper and lower rotor inflow response due to thrust excitation applied to the upper rotor. The corresponding frequency responses for lower rotor thrust excitation are shown in Figure 17. The isolated rotor  $\lambda_o/C_T$  response is shown for reference. The trim thrust coefficient for the isolated rotor case is approximately the same as the total thrust coefficient for the coaxial rotor system ( $C_{T_o} = 0.0067$ ). For upper rotor excitation (Figure 16), the amplitude of the upper and lower rotor inflow response is similar to the isolated rotor case with slightly higher steady state gain for the upper rotor due to the smaller trim thrust coefficient. The phase response for the lower rotor suggests a lag between the inflow and thrust input. When the thrust excitation is applied to the lower rotor (Figure 17), the upper rotor inflow response amplitude is reduced approximately by a factor of 2 (6 dB). This result is consistent with other published results (Ref. 9).

Additional insight into the coaxial rotor system inflow dynamics can be obtained by examining the frequency responses relating the upper and lower inflow responses. These responses are illustrated in Figure 18. For the  $\lambda_{o_l}/\lambda_{o_u}$  relationship (lower rotor inflow due to upper rotor inflow and thrust excitation), the response can be characterized by a pure time delay over the frequency range to approximately 20 rad/sec. Above 20 rad/sec, other wake dynamics may be present but are difficult to characterize due to the low coherence. For the  $\lambda_{o_u}/\lambda_{o_l}$  relationship (upper rotor inflow due to lower rotor inflow and thrust excitation), there is less phase lag, and inflow responses for both rotors appear to be in phase.

In addition, the magnitude comparison in Figure 18 shows that the main inflow interference is that of the lower rotor in a climb with the velocity of the upper rotor (0 db). The interference of the lower rotor on the upper rotor is reduced approximately by a factor of 2. This observation leads to a typical simple modeling assumption for coaxial rotor configurations (Ref. 22).

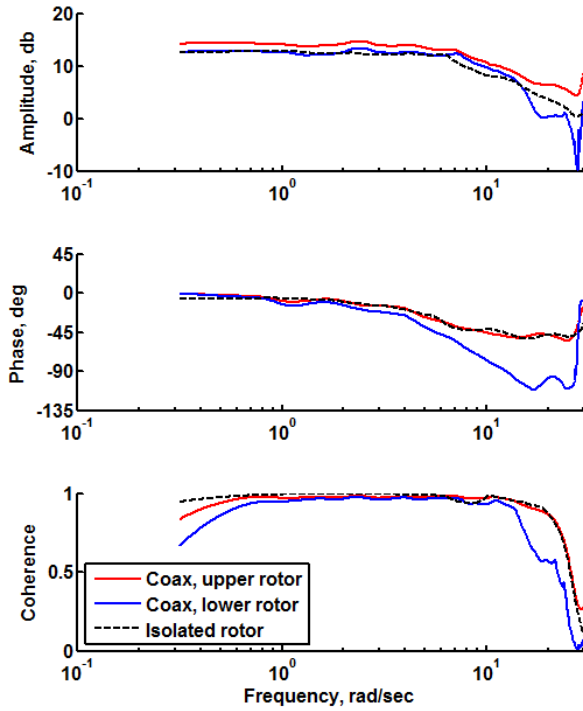


Figure 16. CHARM  $\lambda_0/C_T$  Frequency Sweep, Upper Rotor Excitation, Hover

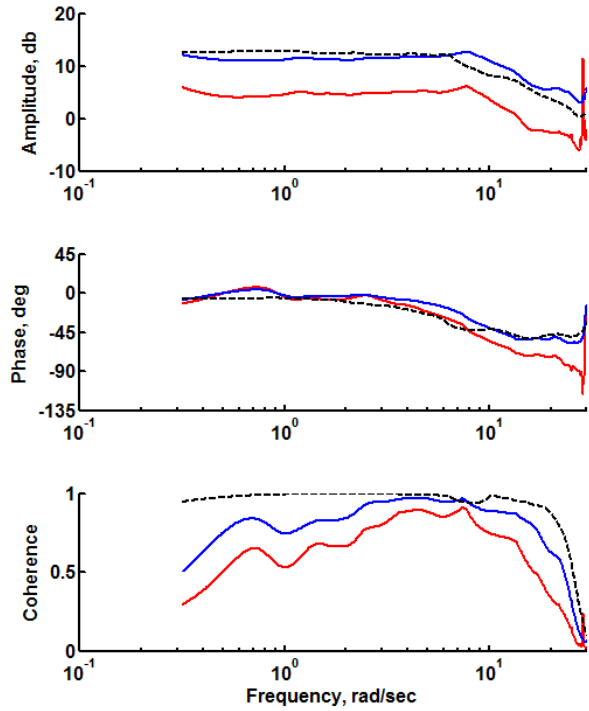


Figure 17. CHARM  $\lambda_0/C_T$  Frequency Sweep, Lower Rotor Excitation, Hover (Legend same as Figure 16)

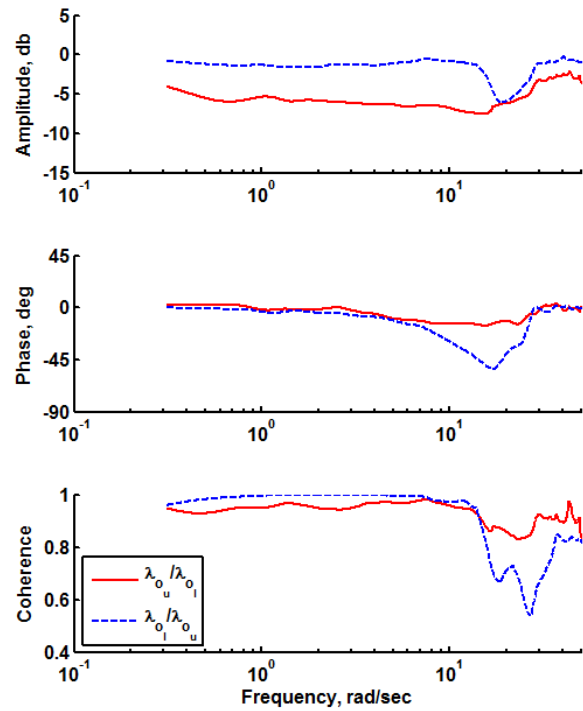


Figure 18. Coaxial Rotor-on-Rotor Frequency Responses, Hover

## Linearized Inflow Model Identification

A linearized inflow model for the coaxial rotor system was determined from the CHARM frequency responses shown in Figure 16 through Figure 18. The model identification considered the uniform inflow response for both rotors due to thrust inputs. Although it is not reported in this paper, the coaxial harmonic inflow response has similar characteristics so that the method described below can be generalized to all three inflow state components.

Two inflow model structures were considered as part of the model identification process. The first model, referred to as “state coupled”, was similar to the form used in Ref. 9 and is a generalization of Eq. (1):

$$\begin{bmatrix} M_{uu} & M_{ul} \\ M_{lu} & M_{ll} \end{bmatrix} \begin{bmatrix} \dot{\lambda}_{ou} \\ \dot{\lambda}_{ol} \end{bmatrix} + \begin{bmatrix} L_{uu} & L_{ul} \\ L_{lu} & L_{ll} \end{bmatrix}^{-1} \begin{bmatrix} \lambda_{ou} \\ \lambda_{ol} \end{bmatrix} = \begin{bmatrix} C_{Tu} \\ C_{Tl} \end{bmatrix} \quad (5)$$

The second model structure can be viewed as an extension of the approach for modeling off-rotor interference effects and is referred to as the “output coupled” model. For this model structure, the inflow through each rotor is determined from the response due to its own loading and the inflow from the other rotor accounting for the delay/transfer function dynamics:

$$\begin{aligned} \lambda_{ou} &= \tilde{\lambda}_{ou} + \tilde{\lambda}_{ol} H_l^u(s) \\ \lambda_{ol} &= \tilde{\lambda}_{ol} + \tilde{\lambda}_{ou} H_u^l(s) \end{aligned} \quad (6)$$

where

$$\begin{aligned} \tau_u \dot{\tilde{\lambda}}_{ou} + \tilde{\lambda}_{ou} &= L_{uu} C_{Tu} \\ \tau_l \dot{\tilde{\lambda}}_{ol} + \tilde{\lambda}_{ol} &= L_{ll} C_{Tl} \end{aligned} \quad (7)$$

with  $\tau_u \equiv L_{uu} M_{uu}$  and  $\tau_l \equiv L_{ll} M_{ll}$ . The form of the inflow transfer functions ( $H_l^u$ ,  $H_u^l$ ) was determined based on the frequency responses in Figure 18. For the lower rotor inflow due to the upper rotor, the transfer function can be represented by a gain and time delay:

$$H_u^l = K_1 e^{-T_u s} \approx K_1 \frac{-s + \frac{2}{T_u}}{s + \frac{2}{T_u}} \quad (8)$$

For the upper rotor inflow due to the lower rotor, the transfer function can be approximated by a gain  $H_l^u \approx K_2$ . Inspection of the above model structures indicates that the output-coupled form has seven free parameters versus eight for the state-coupled form. Thus, parameter correlation can be

expected for model identification using the structure given by Eq. (5), which was confirmed using the CIPHER<sup>®</sup> parameter identification methods.

Identified model results for the coaxial rotor in hover are summarized in Table 9. Included for comparison are coaxial inflow model parameters from Ref. 9, although these results were obtained for a different coaxial rotor system. For the state-coupled model form (Eq. 5), it was found that the model was over-parameterized, and the off-diagonal terms in the inflow mass matrix were set to zero as part of the identification process. The on-diagonal terms of the identified inflow mass matrix for the state-coupled model form were smaller in magnitude and had greater uncertainty than the output-coupled form. The on-diagonal terms of the static gain matrix were similar for both model structures. It can be shown that the off-diagonal terms and inflow transfer function gains ( $K_1$ ,  $K_2$ ) give similar steady state responses.

The addition of the time delay in the lower-to-upper rotor inflow transfer function (Eq. 8) generally improves the frequency response fit primarily for the off-diagonal responses ( $\lambda_{ol}/C_{Tu}$ ,  $\lambda_{ou}/C_{Tl}$ ), which is reflected by the lower average cost function value. This improvement is more significant for the lower rotor inflow response due to the upper rotor thrust (Figure 19). A slight improvement is also seen in the upper rotor inflow due to lower rotor thrust (Figure 20). Note that the primary responses ( $\lambda_{ou}/C_{Tu}$ ,  $\lambda_{ol}/C_{Tl}$ ) are generally unaffected by the inflow time delay.

**Table 9. Identified Coaxial Inflow Model Parameters**

Parameter	Model from Ref. 9	State Coupled Form (Eq. 5)	Output Coupled Form (Eqs. 6-8)
$M_{uu}$	1.07	0.397 (11%)	0.566 (7.2%)
$M_{ll}$	1.02	0.355 (16%)	0.561 (8.4%)
$M_{ul}$	-0.574	0 <sup>†</sup>	---
$M_{lu}$	-0.406	0 <sup>†</sup>	---
$L_{uu}$	5.70	5.10 (3.9%)	5.15 (4.2%)
$L_{ll}$	4.46	4.04 (4.0%)	3.92 (4.3%)
$L_{ul}$	3.52	1.96 (4.5%)	---
$L_{lu}$	4.76	4.32 (4.0%)	---
$K_1$	---	---	0.842 (5.4%)
$K_2$	---	---	0.474 (6.0%)
$T_u$	---	---	0.0475 (18%)
Ave. cost	---	32.0	22.6

<sup>†</sup> Parameter fixed during identification process

To provide verification of the identified inflow models, in addition to an assessment of the significance of model structure differences, predictions of the flap coning and thrust dynamic responses were made and compared with similar results using CHARM for a representative coaxial rotor system. The models were used to predict the flapping response due to a  $\pm 1$ -deg differential collective input, which is relevant for assessing blade separation during a directional input command. Figure 21 compares the flap coning response for the identified inflow models with the corresponding results using the CHARM stand-alone analysis (note that rotor properties were identical to those used for isolated rotor analysis summarized in Table 8). The corresponding thrust response is shown in Figure 22. An approximate model accounting for the aerodynamic lag due to the unsteady near shed wake was included with the identified models. This physical effect is present in the CHARM analysis but not captured by the identified model structure. It can be seen that the identified models over-predict the steady state flapping response but approximately capture the peak response as compared to the CHARM stand-alone analysis. In addition, the identified model structure only appears to affect the peak response and has little effect on the predicted steady state response. This analysis will be extended to the cyclic flapping response to determine if the specific model structure used for coaxial inflow model extraction is critical in hover or forward flight conditions.

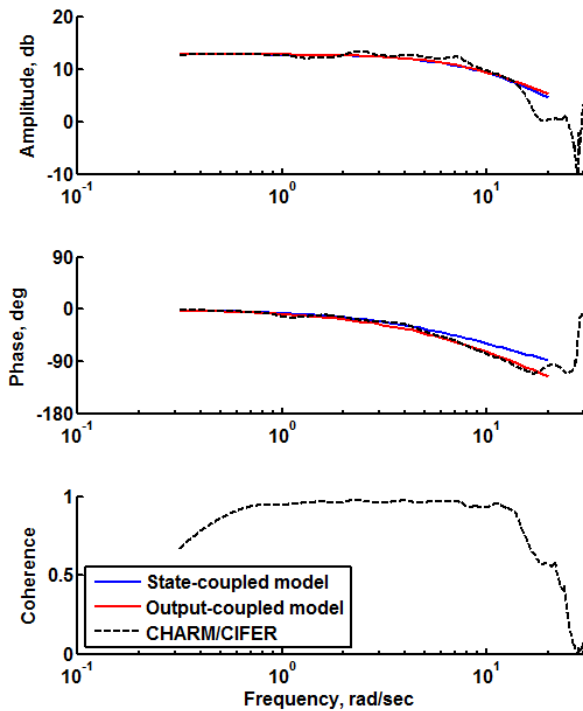


Figure 19. Comparison of Identified Models for Coaxial Lower Rotor Inflow to Upper Rotor Thrust

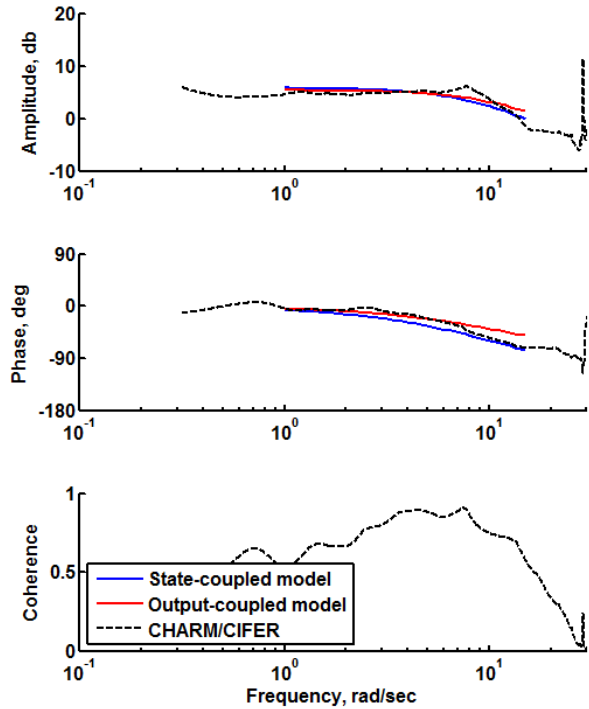


Figure 20. Comparison of Identified Models for Coaxial Upper Rotor Inflow to Lower Rotor Thrust

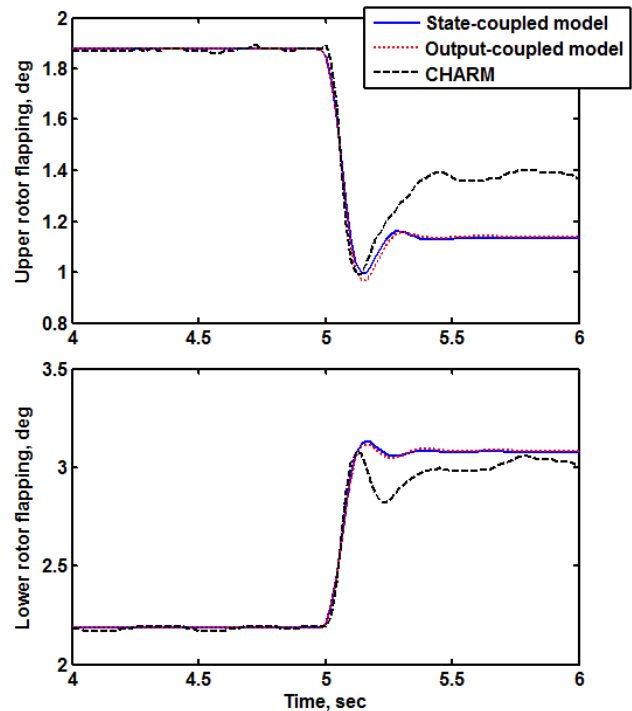


Figure 21. Coupled Flap/Inflow Response for Coaxial Rotor System for Differential Collective Input

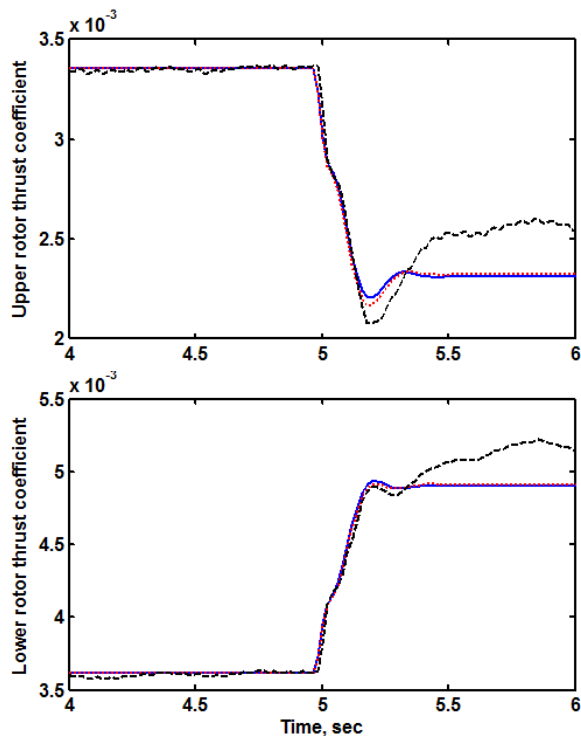


Figure 22. Coaxial Rotor System Thrust Response for Differential Collective Input

## CONCLUSIONS

A linearized inflow model extraction procedure has been developed using free wake analysis and frequency domain parameter identification methods. Extraction of low-order state-space models from comprehensive rotorcraft analyses allows flight dynamics analysis, simulation, and control law development to benefit from the higher fidelity for modeling advanced rotorcraft configurations based on multi-rotor and/or rotor-and-wing compound aircraft. The procedure was demonstrated using the CHARM free wake model and CIFER<sup>®</sup> frequency domain identification method to determine and verify identified model structures. The following specific conclusions can be drawn from this work:

1. Inflow models based on a conventional three-state formulation and extracted using the CHARM/CIFER analysis were found to provide consistent estimates of model parameters for an isolated rotor in hover and forward flight with theoretical predictions and similar published results in the literature.
2. Additional dynamic states and/or time delays are often needed to capture higher-order dynamics associated with the rotor free wake and induced velocity beyond the conventional three-state first order model formulation. Most notable was the second-order behavior of the harmonic inflow response due to aerodynamic loading and tip path plane angular rate in hover. Similar inflow/wake dynamics also may be important in the low speed

forward flight transition regime, as reflected by the uncharacteristically large time delay needed to improve the model fit of cosine harmonic inflow due to thrust inputs.

3. Modeling rotor wake interference at aerodynamic control points away from the rotor and rotor-to-rotor interactions for coaxial rotor systems can be done by accounting for the inflow transfer function, which typically can be modeled as a gain plus time delay. This approach was shown to capture observed behavior from the higher fidelity free wake analysis. Analysis was performed to assess the importance of the induced velocity field dynamics on the flapping response of a coaxial rotor system, and it was found that the response was not strongly affected by the inflow model structure.

Work continues on the development and implementation of an automated procedure to extract linear inflow models from higher fidelity comprehensive analyses. This development will focus on application and validation to both conventional helicopter and advanced rotorcraft configurations based on coaxial and coaxial-compound aircraft designs.

Author contact:

Jeffrey Keller [jeff@continuum-dynamics.com](mailto:jeff@continuum-dynamics.com)

Robert McKillip [bob@continuum-dynamics.com](mailto:bob@continuum-dynamics.com)

Daniel Wachspress [dan@continuum-dynamics.com](mailto:dan@continuum-dynamics.com)

## ACKNOWLEDGMENTS

This work was supported by an SBIR Phase I project for the U.S. Army (Contract No. W911W6-16-C-0001), Dr. Mahendra Bhagwat serving as technical monitor.

## REFERENCES

- <sup>1</sup>Curtiss, H.C., Jr., "Stability and Control Modeling," 12<sup>th</sup> European Rotorcraft Forum, Garmisch-Partenkirchen, West Germany, September 1986.
- <sup>2</sup>Pitt, D.M. and Peters, D.A., "Theoretical Prediction of Dynamic Inflow Derivatives," *Vertica*, Vol. 5, (1), 1981, pp. 21-34.
- <sup>3</sup>Peters, D.A. and He, C., "Correlation of Measured Induced Velocities with a Finite-State Wake Model," *Journal of the American Helicopter Society*, Vol. 36, (3), July 1991, pp. 59-70.
- <sup>4</sup>Keller, J.D., Wachspress, D.A., and Hoffler, J., "Real Time Free Wake and Ship Airwake Model for Rotorcraft Flight Training Application," American Helicopter Society 71<sup>st</sup> Annual Forum, Virginia Beach, VA, May 2015.
- <sup>5</sup>Johnson, W., "Feasibility Investigation of General Time-Domain Unsteady Aerodynamics of Rotors," NASA CR-177570, 1990.
- <sup>6</sup>Celi, R., "State Space Representation of Vortex Wakes

by the Method of Lines,” *Journal of the American Helicopter Society*, Vol. 40, (2), April 2005, pp. 195-205.

<sup>7</sup>Betoney, P., Celi, R., and Leishman, J., “The State-Space Free-Vortex Wake: A Control-Oriented Model,” American Helicopter Society 66<sup>th</sup> Annual Forum, Phoenix, AZ, May 2010.

<sup>8</sup>Rand, O., Khromov, V., Hersey, S., Celi, R., Juhasz, O., and Tischler, M., “Linear Inflow Model Extraction from High-Fidelity Aerodynamic Models for Flight Dynamics Applications,” American Helicopter Society 71<sup>st</sup> Annual Forum, Virginia Beach, VA, May 2015.

<sup>9</sup>Rand, O. and Khromov, V., “Free Wake Based Dynamic Inflow Model in Hover, Forward, and Maneuvering Flight,” American Helicopter Society 72<sup>nd</sup> Annual Forum, West Palm Beach, FL, May 2016.

<sup>10</sup>Quackenbush, T.R., Wachspress, D.A., Keller, J.D., Boschitsch, A.H., Wasileski, B.J., and Lawrence, T.H., “Full Vehicle Flight Simulation with Real Time Free Wake Methods,” AHS Aerodynamics, Acoustics, and Test and Evaluation Technical Specialists Meeting, San Francisco, CA, January 2002.

<sup>11</sup>Wachspress, D.A., Quackenbush, T.R., and Boschitsch, A.H., “First-Principles, Free-Vortex Wake Model for Helicopters and Tiltrotors,” American Helicopter Society 59<sup>th</sup> Annual Forum, Phoenix, AZ, May 2003.

<sup>12</sup>Wachspress, D.A., Keller, J.D., Quackenbush, T.R., Whitehouse, G.R., and Yu, K., “High Fidelity Rotor Aerodynamic Module for Real Time Rotorcraft Flight Simulation,” American Helicopter Society 64<sup>th</sup> Annual Forum, Montreal, Canada, April 2008.

<sup>13</sup>Tischler, M.B., and Remple, R.K., *Aircraft and Rotorcraft System Identification, Second Edition*, AIAA Education Series, Reston, VA, 2012.

<sup>14</sup>Chen, R.T.N., “A Survey of Nonuniform Inflow Models for Rotorcraft Flight Dynamics and Control Applications,” NASA TM 102219, 1989.

<sup>15</sup>Keller, J.D., “An Investigation of Helicopter Dynamic Coupling Using an Analytical Model,” *Journal of the American Helicopter Society*, Vol. 41, (4), October 1996, pp. 322-330.

<sup>16</sup>Curtiss, H.C., Jr., “Aerodynamic Models and the Off-Axis Response,” American Helicopter Society 55<sup>th</sup> Annual Forum, Montreal, Canada, May 1999.

<sup>17</sup>Zhao, J., “Dynamic Wake Distortion Model for Helicopter Maneuvering Flight,” Ph.D. Thesis, Georgia Institute of Technology, March 2005.

<sup>18</sup>Rosen, A. and Isser, A., “A New Model of Rotor Dynamics during Pitch and Roll of a Hovering Helicopter,” *Journal of the American Helicopter Society*, Vol. 40, (3), July 1995, pp.17-28.

<sup>19</sup>Keller, J.D., “The Effect of Rotor Motion on the Induced Velocity in Predicting the Response of Rotorcraft,” Ph.D. Thesis, Princeton University, January 1998.

<sup>20</sup>Johnson, W., *Helicopter Theory*, Princeton University Press, Princeton, NJ, 1980.

<sup>21</sup>Curtiss, H.C., Jr. and Quackenbush, T.R., “The Influence of the Rotor Wake on Rotorcraft Stability and Control,” 15<sup>th</sup> European Rotorcraft Forum, Amsterdam, the Netherlands, September 1989.

<sup>22</sup>Fegely, C., Juhasz, O., Xin, H., and Tischler, M.B., “Flight Dynamics and Control Modeling with System Identification Validation of the Sikorsky X2 Technology™ Demonstrator,” American Helicopter Society 72<sup>nd</sup> Annual Forum, West Palm Beach, FL, May 2016.